International Journal of Coal Geology 86 (2011) 357–366

Contents lists available at ScienceDirect

International Journal of Coal Geology

journal homepage: www.elsevier.com/locate/ijcoalgeo

Stress–damage–flow coupling model and its application to pressure relief coal bed methane in deep coal seam

T.H. Yang [a,*], T. Xu [a,b], H.Y. Liu [c], C.A. Tang [a], B.M. Shi [d], Q.X. Yu [e]

[a] Center for Rock Instability & Seismicity Research, Northeastern University, Shenyang 110004, PR China
[b] State Key Laboratory of Geo-hazard Prevention and Geo-environment Protection, Chengdu University of Technology, Chengdu 610059, PR China
[c] School of Engineering, the University of Tasmania, Hobart TAS7001, Australia
[d] School of Energy and Safety Engineering, Anhui University of Science and Technology, Huainan 232001, PR China
[e] School of Safety Engineering, China University of Mining and Technology, Xuzhou 221116, PR China

ARTICLE INFO

Article history:
Received 2 August 2010
Received in revised form 10 April 2011
Accepted 11 April 2011
Available online 16 April 2011

Keywords:
Gas permeability
Numerical simulation
Stress-damage-flow coupling
Pressure relief gas drainage

ABSTRACT

Long-distance pressure relief gas drainage technology has recently been applied in mining areas with multiple coal seams of low permeability in China. This study briefly described a coupled stress–damage–flow model, which combined the evolution of stress, damage, and gas permeability with the deformation of coal and rock. The coupled model was then used to investigate the deformation and fracture characteristics of overburden strata, the evolution of gas permeability and gas flow in target coal seams. The effectiveness of long-distance pressure relief gas drainage was evaluated on the basis of the calculated results from a dynamic modelling of extraction of protective coal seam at great depths. The numerical results revealed that the stress was remarkably relieved in the target coal seam above 67 m away from the coal seam being mined. Moreover, the range of stress relief extended above 70 m and the gas permeability increased by more than 2000 times. The modelled results reasonably well agreed with the field results observed in the PANYI coal mine. It was concluded that the long-distance pressure relief gas drainage technology could effectively improve the safety and productivity in underground coal mines, especially in mining areas with multiple coal seams of low permeability.

1. Introduction

Underground coal mining has been considered a high risk activity worldwide. Violent roof failure or coal and gas outbursts induced by coal mining have always been a serious threat to the safety and efficiency of coal mines in China. A great number of accidents have taken place throughout history in coal mines of this kind, leading to the loss of human lives in many cases. Most of these accidents are induced by gas released from coal seams. Gas release is potentially dangerous when encountered in sufficient quantities in the coal seam, not only due to the explosive risk but also the risk of coal and gas outburst. There are many serious gas accidents, which results in numerous casualties in each year in China. With the depth and intensity of coal mining increasing, the possible occurrence of gas disasters in coal mines poses a great potential threat to underground coal mining.

In recent years, a new mining technique called pressure relief gas drainage technology has been applied in mining areas with multiple high-gassy coal seams of low gas permeability (Chen et al., 2004; Yu et al., 2004). The main idea of the technique is to first mine the coal seam with low gas contents and low-risks of coal and gas outburst, which serves to relieve the stress in the protected coal seam and improve the gas permeability of the protected coal seam. Furthermore, the technique promotes considerably the desorption of coal methane in protected coal seam and the formation of a high-efficiency extraction conditions, which facilitates the subsequent gas drainage in protected target coal seam. Correspondingly, the technique not only avoids the pollution of air by gas released from coal seams and gob, but also greatly reduces the gas content in the coal seams to eliminate the danger of gas explosion and coal and gas outburst. Thus, the technique secures a fast and high-efficiency exploitation of gas and coal in the pressure relieved coal seams.

The pressure relief gas drainage technology is used too in mining areas with multiple high-gassy coal seams in many countries (such as Russia, USA, Germany, Britain, Australia, Poland, and Ukraine) to control gas emission of the upper coal seams during multiple coal seams mining. For a mining height of 1.3–2.0 m, the distance between the pressure relief coal seam and underlying coal seam being extracted is usually no more than 50 m, and the relative coal seam distance is normally less than 25–30. The relative coal seam distance is defined as the ratio of the normal distance between the pressure relief coal seam and the protective coal seam to the thickness of the

* Corresponding author. Tel./fax: +86 24 83681889.
E-mail address: yang_tianhong@126.com (T.H. Yang).

0166-5162/$ – see front matter © 2011 Elsevier B.V. All rights reserved.
doi:10.1016/j.coal.2011.04.002

protective coal seam, which is used to describe the pressure relief degree. For example, the maximum relative coal seam distance in Germany, USA, Ukraine, and Russia are 37, 33, 37.5 and 35, respectively (Huainan Mining Group, 2002; Noack, 1998; Schneider and Preuße, 1995). Moreover, it is suggested that the spacing of two target coal seams exceeding 70 m is unfavorable. Russia and the European Community carried out a systematical investigation on the pressure relief gas drainage in multiple coal seams and made some invaluable achievements in the drainage method and drainage parameters. Though great progress has been made in recent years, there is limited work on the application of pressure relief gas drainage in bending zone for pressure relief with a separation of 70 m between two target coal seams. Both theoretical research and engineering practice are needed to investigate for the technique of pressure relief gas drainage, the associated gas flow characteristics in coal seam, and the formulation of coupled solid–gas model for underground coal mining.

It is the theoretical basis of implementing the new mining conception mentioned above to study the gas permeability change in surrounding rock, the gas flow law in coal seam induced by exploitation, and the gas–solid coupled model in the process of exploitation. Currently, considerable efforts have been made to study the evolution of gas permeability, the gas flow law in coal seam, and the coupled effect of coal and gas during coal seam mining through laboratory experiments, numerical simulations, and field tests. Among the work, reviews on the hypothesis and mechanism of coal and gas outbursts were made by some researchers at early stage (Beamish and Crosdale, 1998; Hargraves, 1983; Hyman, 1987; Shepherd et al., 1981). Thereafter some more complex models for coal and gas outburst were proposed to gain insight into the mechanical mechanism of coal seam and gas (Otuonye and Sheng, 1994; Paterson, 1986; Valliappan and Zhang, 1999; Yu, 1992). Considerable efforts were also spent on the mathematical model of coupled solid–gas for gas flow in porous media, the modeling of gas migration and outbursts in coal mines and the efficient recovery of methane from coal seams(Chan et al., 1993; Sun and Wan, 2004; Valliappan and Zhang, 1996; Zhao and Valliappan, 1995). Bauer and Lydzba (1994) presented constitutive equations of a gas–coal two-phase medium with a local mass exchange due to a sorption–desorption phenomenon. As for the change of permeability, Viete and Ranjith (2006) studied the effect of CO_2 on the geomechanical and permeability behaviour of brown coal to be potential for coal seam CO_2 sequestration. Zhu et al. (2007) analyzed the coupled gas flow and deformation process with desorption and Klinkenberg effects in coal seams. Concise relationships were developed for variations of permeability on the basis of the nature of the coal matrix shrinking with gas desorption and swelling with adsorption (Connell, 2009). Recently, the method of pressure relief long-distance gas drainage in thick and high-gassy seams has been experimented in fields for safe and high-efficient exploitation of coal and pressure relief gas (Chen et al., 2004). Although great progress has been made, it is difficult to study the large deformation, dynamic caving process of strata, gas permeability change, and gas flow law, using the existing methods due to the geological complexity of coal seam, overburden strata, and the coupled effect of gas and surrounding stresses during the exploitation.

In this paper, based on mechanical analysis and engineering practice of pressure relief long-distance gas drainage at the PANYI coal mine, in Huainan coal mining Co. Ltd, a coupled stress–damage–flow mathematical model for gassy coal and rock failure is firstly described. Then the extraction of coal seam at great depth with this technique was numerically simulated. On the basis of the modeled results, the deformation and fracture characteristics of overburden strata, the evolution of gas permeability, and the gas migration in target coal seams were analyzed. It is expected throughout this study to gain an insight into the gas flow and migration mechanism and to offer some theoretical basis and scientific evidence for the application of the pressure relief long-distance gas drainage technique.

2. Theoretical model

Numerical model is currently the most commonly used method in the solution of complex problems in rock mechanics and engineering, such as reservoir simulation and coal bed methane recovery (Connell and Detournay, 2009; Karacan et al., 2007; Lunarzewski, 1998; Pan and Connell, 2009; Xu et al., 2007). In this paper, a quantitative model, i.e. the two-dimensional Rock Failure Process Analysis for Gas Flow model (abbreviated as RFPA^{2D}-GasFlow) (Xu et al., 2006; Yang et al., 2004), was proposed to describe the coupled gas flow and rock failure problems associated with coal seam mining. The model was then applied to investigate the mechanism of the complex gas migration during coal mining intending to gain an insight into the coupling mechanism between gas flow and coal deformation.

When the model is formulated in mathematical language, various levels of complexity can be incorporated into each component, with the accuracy and versatility of the model depending on the refinement of the components description. For porous medium like coal seam, the coupled effect of the medium deformation and fluid flow may be important to be formulated. The formulation of the coupled model may help understand the mechanism of gas migration in gas drainage, coal and gas outbursts in mining or drilling and gas disposal in engineering practice. As we know, for a model that can be used to describe the coupling effect between gas flow and coal deformation, three components must be accounted for: (i) a gas flow description, (ii) a stress description, and (iii) a failure description. Hereby, the gas flow, the stress analysis, and the failure criterion, which are implemented in the RFPA^{2D}-GasFlow model, are presented in the following sections.

2.1. Gas flow

The fundamental assumption in the stress–damage–flow model presented here is that the coal is saturated with gas. Thus the equations for two-phase flow in porous media should be used. In 1856, Henry Philibert Gaspard Darcy (Hubbert, 1957) first developed the equation to describe fluid flow through a porous media. Based on the Darcy's Law, Zhou and Lin (1998) further developed the gas filtration equation followed by linear law in Eq. (1) (see Appendix A).

$$q_i = -\lambda_{ij}\frac{dP}{dn} \tag{1}$$

where, q_i denotes gas filtration rate ($i=1, 2, 3$) in m/s; λ_{ij} is coefficient of gas filtration (i , $j=1, 2, 3$) in m^2/(MPa^2 S); and P is square of gas pressure in MPa^2. Normally, the coefficient of gas filtration λ_{ij} is about 2.5×10^{-17} m^2 times that of the intrinsic permeability k in value. Note that the parameters λ_{ij} and P is different from those in Darcy's law though they are similar in form, as shown in Appendix A.

Generally, gas occurs in coal as two distinct forms, free gas and adsorbed gas. The adsorbed gas typically accounts for over 95% of the total gas, depending on the pressure at which the gas is adsorbed. The free gas, only a little fraction of the total gas, is stored in the pores or cleats either free or in solution. The total gas content in coal can be approximated by empirical relationship in Eq. (2) (Zhou and Lin, 1998)

$$X = A\sqrt{p} \tag{2}$$

where, X is gas content in gassy coal in m^3/m^3; A is the empirical coefficient of gas content in m^3/(m^3 MPa$^{1/2}$), and p is gas pressure in MPa.

According to the fundamental seepage theory of gas flow in porous media, the isothermal filtration gas flow in gassy coal and rock can be described as Eq. (3)

$$\alpha_p \cdot \nabla^2 P = \frac{\partial P}{\partial t} \tag{3}$$

where, $\alpha_p = 4\lambda A^{-1} P^{\frac{3}{4}}$.

2.2. Stress analysis

The stress calculations can be formulated in a number of ways. For a stress analysis in terms of effective stress, the stress equilibrium equations take the form

$$\sigma_{ij,j} + f_i = 0 \tag{4}$$

where, σ_{ij} is stress tensor, $(i, j = 1, 2, 3)$ in MPa; f_i is stress caused by the body forces per unit volume in MPa.

On the basis of Terzaghi's effective stress principle (Terzaghi et al., 1996), the stress equilibrium equation can be expressed as Eq. (5) for one- to two-phase materials:

$$\sigma_{ij} = \sigma'_{ij} + \alpha \cdot p \cdot \delta_{ij} \tag{5}$$

where, σ_{ij} is the total stress tensor; σ'_{ij} is the effective stress tensor of the solid phase; p is the gas pressure; α is a positive constant, which is equal to 1 when individual grains are much more incompressible than the grain skeleton; and δ_{ij} is the Kronecker delta function.

Substitution of Eq. (5) into Eq. (4) leads to Eq. (6) as follows:

$$\sigma'_{ij,j} + f_i + \left(\alpha \cdot p \cdot \delta_{ij}\right)_{,j} = 0 \tag{6}$$

The equilibrium equation is then expressed according to the effective stress principle.

According to the continuous conditions, for a perfectly elastic isotropic continuum, the geometrical equation can be expressed as Eq. (7)

$$\varepsilon_{ij} = \frac{1}{2}\left(u_{i,j} + u_{j,i}\right) \tag{7}$$

where, ε_{ij} is strain tensor, $(i,j = 1, 2, 3)$; ε_v is the volumetric strain; $\varepsilon_v = \varepsilon_{11} + \varepsilon_{22} + \varepsilon_{33}$; and u is the displacement of element.

The constitutive equation of deformation fields can be expressed as Eq. (8) for elastic isotropic materials.

$$\sigma'_{ij} = K\delta_{ij}\varepsilon_v + 2G\varepsilon_{ij} \tag{8}$$

where, G is shear modulus and K is Lame's constant.

On the basis of the equilibrium (Eq. (6)), continuity (Eq. (7)), and constitutive (Eq. (8)) equations, the governing equations can be represented as Eq. (9) for mathematical model of coal/rock deformation considering the gas pressure in coal/rock:

$$(K + G) \cdot u_{j,ji} + G u_{i,jj} + f_i + (\alpha \cdot p)_{,i} = 0 \tag{9}$$

2.3. Stress induced permeability evolution

Generally, the stress decrease is the main factor leading to the increase of the gas permeability. In the numerical model, gas flow is coupled to stress describing the permeability change induced by the decrease of the stress field. The coupling function can be described as Eq. (10) (Louis, 1974):

$$\lambda / \lambda_0 = e^{-\beta\sigma'} \tag{10}$$

where, λ is current gas permeability; λ_0 is original gas permeability; β is coupling coefficient (stress sensitive factor to be measured by experiment); and σ' is effective stress. Fig. 1 shows the evolution of the permeability coefficient, which indicates that the larger the parameter β is, the greater the range of stress induced permeability.

2.4. Damage induced permeability evolution

In the model, only elastic constitutive law with linear behaviour has been introduced for all elements, which have been assigned to have different strength and elastic constant parameters depending on the heterogeneity of rock materials. When the stress of the element satisfies the strength criterion (such as the Coulomb–Mohr criterion), the element begins to undergo damage. In elastic damage mechanics, the elastic modulus of the element may degrade gradually as damage progresses. If the element and its damage are assumed to be isotropic, the elastic modulus of the damaged element is defined as follows (Lemaitre and Desmorat, 2005):

$$E = E_0(1-D) \tag{11}$$

where, D represents the damage variable, and E and E_0 are the elastic moduli of the damaged and undamaged elements, respectively. The parameters E, E_0, and D are all scalar.

Under compression states, the Mohr–Coulomb criterion is chosen as the strength criterion for the elements:

$$\sigma_1 - \sigma_3 \frac{1 + \sin\phi}{1 - \sin\phi} \geq f_c \tag{12}$$

where, $\sigma_1$and σ_3 are the maximum principal stress and minimum principal stress, respectively, ϕ is the internal friction angle, and f_c is the threshold of the compressive strength of the element.

Correspondingly, the damage variable D in compression can be expressed as (Tang et al., 2002):

$$D = \begin{cases} 0 & \varepsilon < \varepsilon_{c_0} \\ 1 - \dfrac{f_{cr}}{E_0 \varepsilon} & \varepsilon_{c_0} \leq \varepsilon \end{cases} \tag{13}$$

where, f_{cr} is the residual compressive strength; ε and ε_{c_0} are the compressive strain and the compressive threshold strain, respectively.

Similarly, the maximum tensile stress criterion is chosen as the strength criterion for the elements in tension

$$\sigma_3 \leq -f_t \tag{14}$$

where, f_t is the threshold of the tensile strength of the element.

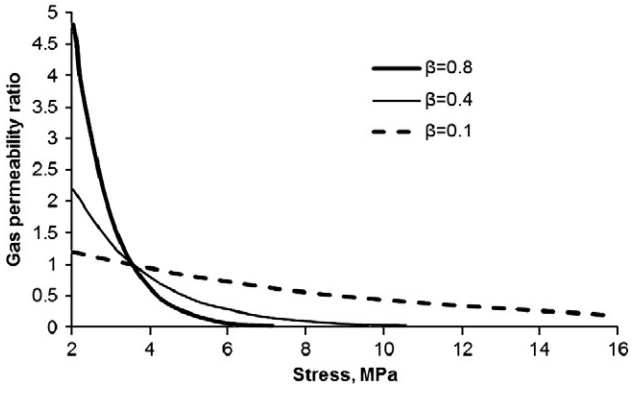

Fig. 1. Gas permeability versus stress under different coupling parameters β.

Correspondingly, the damage variable D in tension can be expressed as

$$D = \begin{cases} 0 & \varepsilon_{t_0} \le \varepsilon \\ 1 - \dfrac{f_{tr}}{E_0 \varepsilon} & \varepsilon_{t_u} \le \varepsilon < \varepsilon_{t_0} \\ 1 & \varepsilon \le \varepsilon_{t_u} \end{cases} \tag{15}$$

where f_{tr} is the residual tensile strength of the elements; $\varepsilon_{t_0}$and ε_{t_u} are the tensile threshold strain of the damage elements and the ultimate tensile strain of the failed elements, respectively.

For damage induced permeability change, most of the theories are only valid in pre-failure regions. During elastic deformations, rock permeability may either decreases when the rock compacts or increases when the rock extends. However, a dramatic and remarkable increase in rock permeability can be expected as a result of the generation of numerous micro fractures while the peak load reaches. Once passing the peak load, the permeability may gradually drop again should the failed rock be further compacted, or the permeability may increase continuously should the failed rock be further extended. The gas permeability coefficients in uniaxial compression and tension can be described as Eqs. (16) and (17), respectively. For the elements in compression, the gas permeability can be described as Eq. (16):

$$\lambda = \begin{cases} \lambda_0 e^{-\beta(\sigma_1 - \alpha p)} & D = 0 \\ \xi \lambda_0 e^{-\beta(\sigma_1 - \alpha p)} & D > 0 \end{cases} \tag{16}$$

where, λ_0 is the initial gas permeability for unloaded coal and rock; β is the coupling factor of stress to pore pressure; α is the coefficient of pore pressure; and ξ is the coefficient of sudden jump of gas permeability for loaded elements in compression.

For the elements in tension, the gas permeability–stress equation is expressed as Eq. (17)

$$\lambda = \begin{cases} \lambda_0 e^{-\beta(\sigma_3 - \alpha p)} & D = 0 \\ \xi \lambda_0 e^{-\beta(\sigma_3 - \alpha p)} & 0 < D < 1 \\ \xi' \lambda_0 e^{-\beta(\sigma_3 - p)} & D = 1 \end{cases} \tag{17}$$

where, ξ' is the coefficient of sudden jump of gas permeability for failed elements in tension.

The other parameters are the same as those in the equations mentioned above. In this way, the damage induced stiffness degradation and damage induced permeability variation were presented in the RFPA^{2D}-GasFlow model. Fig. 2 illustrates the flow chart of the mathematical model.

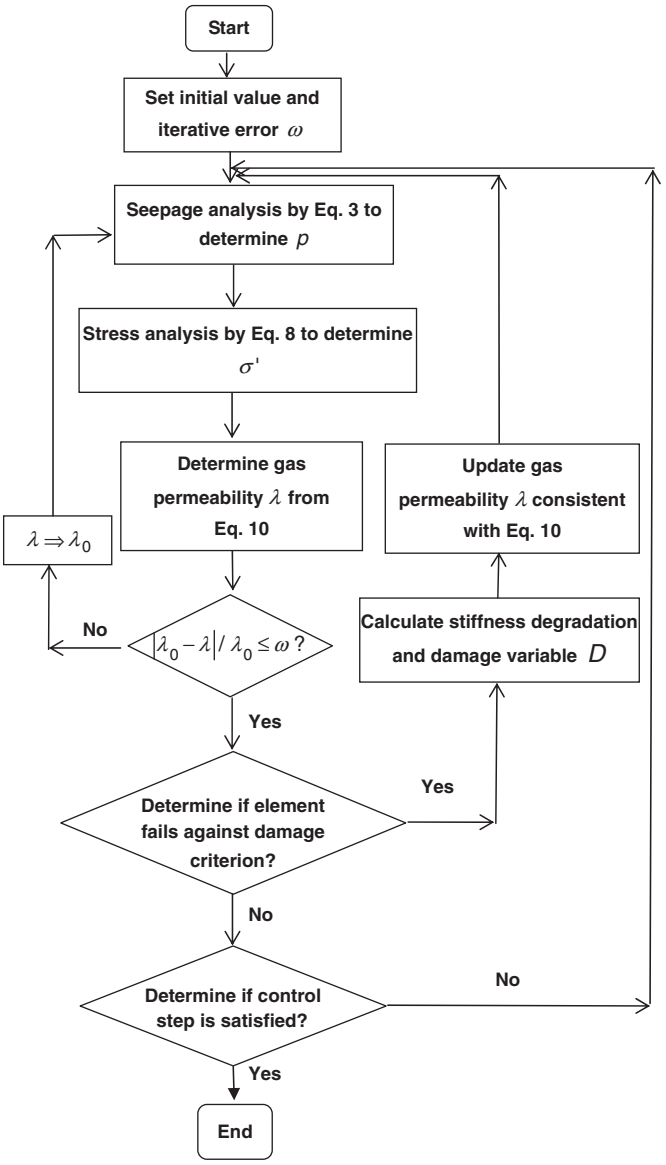

Fig. 2. Flow chart of the numerical model.

3. A case study

3.1. Description of the area under study

The PANYI coal mine of Huainan Mining Group Co. Ltd, is located in the Huainan coal mining area, one of the largest coal fields in China. It has been being mined since 1983. Currently, the annual production capacity is three million tons per year. It is a typical highly gassy mine and considerable attentions should be paid to ensuring mining safety during coal extraction. At present, the coal seams No C_{13}, B_{11}, and B_8 are being mined. The mining level is between −530 m and −650 m. Long-wall mining method is adopted in the coal mine. The zone studied in this paper was in the DONGYI and the DONG'ER mining sections. The planned daily production was 2,000 tons when full-mechanized exploitation was adopted. The initial protective coal seam was the coal seam No B_{11} and the district was the No 2351 working face. The strike and dip length of the working face was 1640 m and 190 m, respectively. The thickness of the coal seam No B_{11} was 1.5–2.4 m, with an average thickness of 2 m. The slope angle of the coal seam was 6–13°, with an average angle of 9°. The original gas content of coal seam No B_{11} is 4–7.5 m^3/t, with an average gas content gradient of 75.7 m/(m^3/t), the relative gas emission of 5.23–7.32 m^3/t, and the absolute gas emission of 3.07–3.38 m^3/min, far below those of coal seam No C_{13}. Thus, the coal seam No B_{11} had no coal and gas outburst danger. The thickness of the coal seam No B_{11} is stable and the geological structure is simple. In contrary, the thickness of the coal seam No C_{13} was 5.57–6.25 m and the average thickness was 6 m. The slope angle of the coal seam varied from 6° to 13° and was 9° on average. The measured gas pressure of the coal seam No C_{13} in this district was about 4.4 MPa on average, with a fluctuation of 5.0 MPa at the level of −580 m and 5.6 MPa at the level of −620 m. The gas content was 14.2 m^3/t and the average gas pressure gradient was 2.42×10 MPa/m. The initial gas permeability coefficient was 2.84×10^{-4} in milli-darcy and gas content coefficient was 9 m^3/m^3 ($MPa^{0.5}$). The gas permeability coefficients of coal and rock are expressed in the international unit of milli-darcy in this paper though they are commonly expressed in m^2/(MPa^2 d) in the coal mines in China. During coal mining, the relative gas emission is 14.8–38.6 m^3/t, with an average gas emission up to 25.0 m^3/t. The absolute gas emission is 22.7–33.1 m^3/min and was 27.0 m^3/min on average. Fig. 3

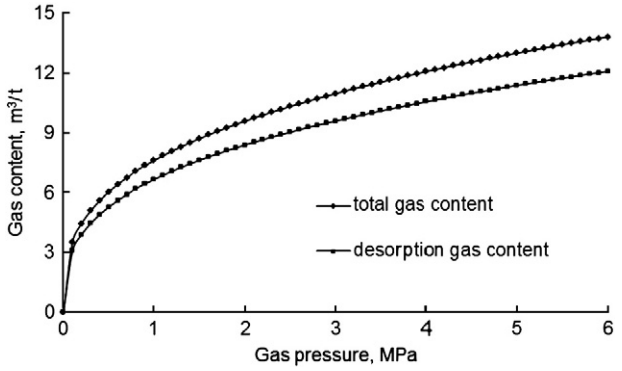

Fig. 3. Relationship between the gas pressure and the gas content of the coal seam No C_{13}.

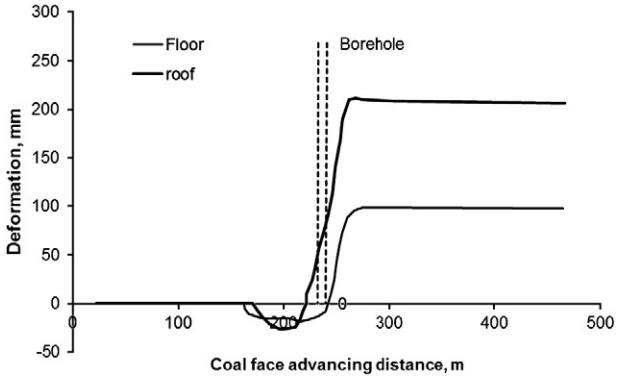

Fig. 4. Deformation of the roof and the floor in the coal seam No C_{13} along the advancing direction of the working face.

shows the relationship between gas pressure and gas content of coal seam No C_{13}. The thickness of the coal seam No C_{13} is stable and the geological structure is simple as well. The strike and dip length of the working face in coal seam No C_{13} was 1680 and 160 m, respectively. Coal and gas outburst and gas explosion accidents have ever frequently occurred in the coal seam No C_{13} in recent years. It was about 67 m away from the roof of the coal seam No B_{11} to coal seam No C_{13} and the relative coal seam distance was 35 m. Due to low gas content of coal seam No B_{11}, and high gas content and low permeability of coal seam No C_{13}, coal seam No B_{11} was first mined to reduce the stress fields and increase the gas permeability of the coal seam No C_{13}. Meanwhile, the pressure relief gas drainage by long-distance boreholes was performed to capture the released gas and avoid possible coal and gas outbursts. In this study, the No 2151 working face of the coal seam No B_{11} was first extracted and the coal seam No C_{13} was considered as the pressure relief coal seam. The No 2121 working face of the coal seam No C_{13} was then worked after the gas permeability of the coal seam No C_{13} was enhanced by the pressure relief induced by the extraction of the coal seam No B_{11}.

3.2. Case study

After the coal seam No B_{11} is mined, the height of the fractured zone measured in field is 30.1–36.1 m, which is formed by horizontal bedding plane separations and vertical mining induced fractures. The height of the caving zone, characterized as fragmented rock mass, is 8.5–11.0 m. The coal seam No C_{13} just lies in the bending zone of the overlying strata induced by coal mining. It is indicated that the extraction of the coal seam No B_{11} only causes the subsidence of the coal seam No C_{13} as a whole, in which parallel layered fissures and a few vertical cross fissures form.

Monitoring points were installed through drilling two boreholes at the top and bottom of gas drainage testing laneway below the coal seam No C_{13} to determine the deformation of coal seam by measuring the relative displacement of two points. Fig. 4 shows the testing curve of the relative displacement between roof and floor in the coal seam No C_{13} along the advancing direction. It can be seen from Fig. 4 that the compressive deformation of both sides of the coal seam No C_{13} is up to 27 mm and the expansive deformation of the coal seam No C_{13} in the centre reaches to 210.44 mm. The largest relative compressive deformation of the coal seam No C_{13} is 3.37‰ and the largest relative expansive deformation is 26.3‰, indicating that the in-situ stress in the coal seam No C_{13} remarkably decreases and correspondingly the fractures in the coal seam No C_{13} considerably increases due to the extraction of the coal seam No B_{11}. In addition, the monitoring points were installed, too, along the floor of the gas drainage testing laneway in the coal seam No C_{13} before mining the coal seam No B_{11}. The final relative displacement of the floor in the coal seam No C_{13} was measured during mining the coal seam No B_{11}. Fig. 5 shows the relationship between the floor subsidence of the coal seam No C_{13} and the mining distance away from the working face obtained through the in-situ testing. It can be seen from Fig. 5 that the subsidence displacement reaches the maximum average value of 1.56 m at about 40 m away from the open-off cut of the working face. On the whole, the support of the roadway is still stable and the roadways in the bending zone are suitable for gas drainage.

Three gas drainage testing boreholes, which lie within the boundary of unloading stress induced by mining coal seam B_{11}, were installed in the coal seam No C_{13} (Fig. 6) to determine the changes of gas pressure, gas flow, and gas permeability with the advance of the working face in the coal seam No B_{11}. As the working face advances, the gas flow in the borehole No.3 reaches to 4.48 L/min (6.45 m^3/d), specific gas flow 1.82 $m^3/(d \cdot m^2)$ and the coefficient of gas permeability 0.284 mD. It is noted that the coefficient of gas permeability increases 2800 times, at the intervals of four and a half days, from the 11:40 am, July 31, 2000 to 10:00 am, August 4, 2000 (Fig. 7). Moreover, Fig. 7 depicted, too, the variation of the gas pressure measured around the borehole in the coal seam No C13 as the working face advances. It can be seen that the gas pressure sharply decrease from 4.4 MPa to 0.4 MPa as the working face advances from about 100 m to 80 m away from the borehole in the coal seam No C13 along the strike projection direction. Subsequently, the gas pressure stabilizes at approximately 0.4 MPa as the working face advances from about 80 m to further away from the borehole.

4. Numerical simulation

4.1. Model setup

According to the in-situ stresses, gas pressures, gas permeability, and other mechanic parameters measured in the field, a plain strain

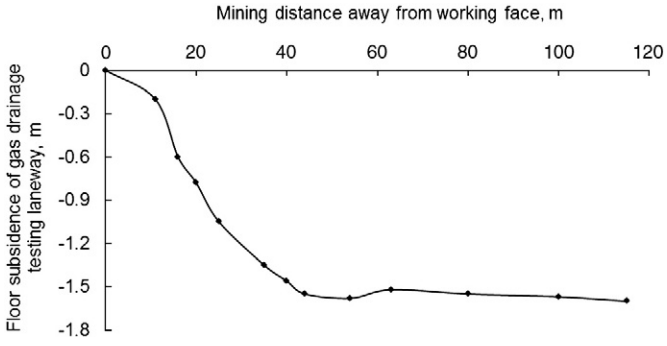

Fig. 5. Relationship between the floor subsidence of the gas drainage testing laneway and the mining distance measured from the working face.

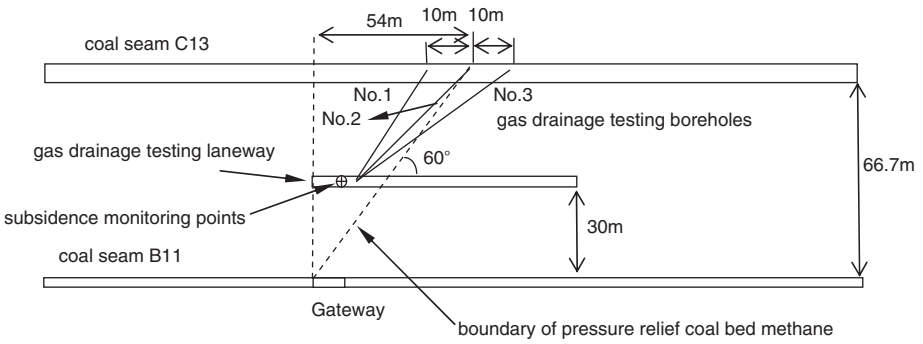

Fig. 6. Position of the gas drainage testing boreholes in the coal seam No C_{13}.

model is setup for the case mentioned above using the RFPA^{2D}-GasFlow code, as shown in Fig. 8. The grayness level in the Fig. 8 represents the magnitude of elastic modulus. The lighter the gray is, the higher the elastic modulus. The domain of the numerical model is 110 m in height and 300 m in length. The thickness of the upper coal seam No C_{13} is 6 m, which is located at 500 m below the earth surface. The pressure of 10 MPa is loaded on the model surface boundary to represent the dead weight of 500 m strata in thickness. The thickness of the coal seam No B_{11}, sixty-seven meters away from the upper coal seam No C_{13}, is 2 m. The numerical model contains a total of 10 layers based on the site-specific geological conditions. With the effect of bedding and weak planes on the failure of rock mass in the mind, it is necessary to embed some bedding planes in the model. The mining length of the coal seam B_{11} is 100 m, which is mined in 20 steps in total, i.e. 5 m per step. In the light of site-specific mining conditions, it is assumed that the time interval of each step is a half day. For example, the extraction of the coal seam No B_{11} lasts 10 days in the simulation. The initial gas pressure in the coal seam No C_{13} is 5 MPa and the initial gas pressure in the strata above and below the coal seam No C_{13} are assumed to be approximately zero, as shown in Fig. 8. The gas drainage hole is located in the middle of the coal seam No C_{13} and its initial gas pressure is 20 kPa. The time interval of drainage at the hole is 0.5 day per step. As the working face advances, the seepage of gas from the coal seam gradually continues. In this model, gas permeability λ at zero stress condition is 0.284 mD, and stress sensitive factor β is 2.0. The physical, mechanical, and seepage parameters in the model are listed in Table 1. The numerical simulation was carried out to investigate the strata deformation and failure, the change of gas permeability and the characteristics of gas flow in the coal seam C_{13} during the extraction of the coal seam B_{11}.

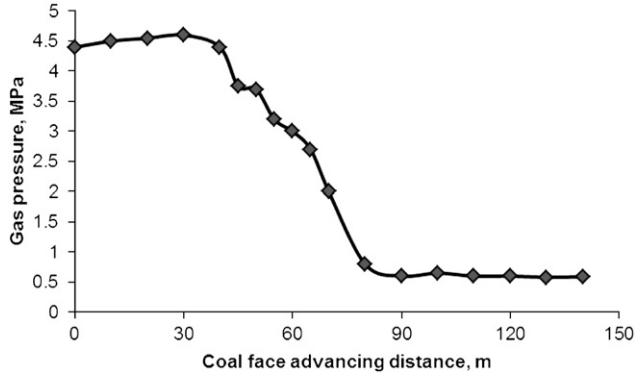

Fig. 7. Variation of the gas pressure around the borehole in the coal seam No C_{13} with the working face advancing.

4.2. Deformation and fracture characteristics of overburden strata

Fig. 9 depicts dynamic evolution of fracturing, caving processes and corresponding stress field evolution in the overburden strata during mining. The grayness levels represent the magnitude of stresses. The lighter the gray is, the higher the stress, and vice versa. It can be seen that, with the working face advancing, the strata above the mined coal seam gradually fracture and cave. Correspondingly, the three zones (i.e., caving, fractured, and bending zones) form in the overburden strata above the mined coal seam. Moreover, the numerical results show that the initial caving spacing is 30 m and sequent periodic caving spacing is about 15 m, which agrees well with the field observations. When the working face advances close to 100 m, the height of the caving zone in the overburden strata above the coal seam No B_{11} is between 15 m and 20 m, and the height of the fractured zone is between 40 m and 45 m. In addition, the results indicate that the extraction of the coal seam No B_{11} does not cause the fracture of the coal seam No C_{13}, but does cause the subsidence of the coal seam No C_{13} since it lies in the mining induced bending zone in the overburden strata.

4.3. Effect of in-situ stress on gas permeability of coal seam

The extraction of the coal seam No B_{11} leads to the redistribution of the stress fields in the overburden strata, which in turn causes the change of gas permeability in the coal seam. Figs. 10 and 11 depict the evolution of stress and gas permeability, respectively, along the horizontal direction of the coal seam No C_{13} with the mining of the coal seam No B_{11}. It can be seen that there is considerably wide changes in the stress and gas permeability. When the working face advances 0.5 day (2.5 m), the ground stress in the protected coal seam No C_{13} decreases slightly. A stress-relief area is produced and the gas permeability of the coal seam increases. However, the range of the stress-relief area is small and the degree of pressure relief is low, indicating that the relief effect on the protected coal seam is small. At the same time, a stress concentration region appears in the protected coal seam. When the working face continuously advances about 7 days (35 m), the overlying coal or rock mass subsides. The stress-relief area of the protected coal seam No C_{13} increases above the goaf, the in-situ stress decreases and the seam permeability further increases. The magnitude and range of the stress concentration also increase slightly. When the coal face is advances to 10 days, the stress-relief area in the protected coal seam further increases and the overburden strata above working face caved. It is found that the magnitude of the gas permeability in the coal seam No C_{13} increases by 2100 times compared to the initial gas permeability. Moreover, the horizontal range of the coal seam with an obvious increase of the gas permeability is up to 70 m when the stress sensitivity factor β is 2.0. The effect of the pressure relief and the increase of the gas

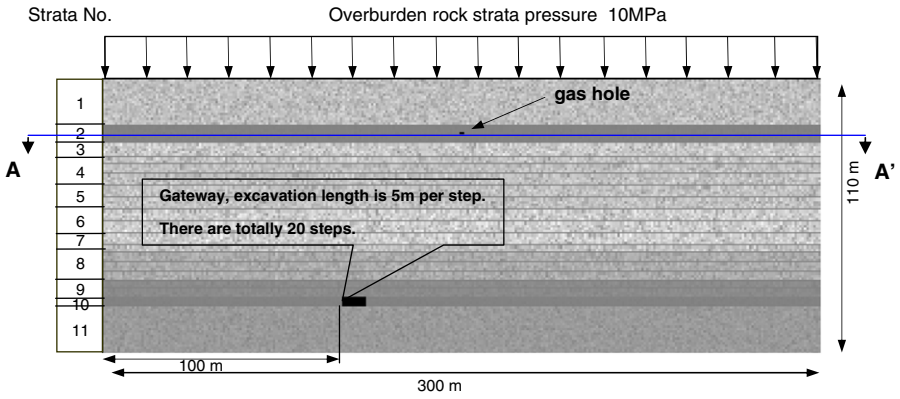

Fig. 8. Numerical model.

permeability are obvious in the protected coal seam No C_{13}. In contrary, when the stress sensitivity factor β is 1.6 but other stress conditions are the same, the magnitude of the gas permeability change in the coal seam No C_{13} is 1000 times, compared to the initial gas permeability and the horizontal range of the coal seam with an obvious increase of the gas permeability is about 50 m. It is concluded that the stress sensitivity factor β is an important factor for modeling the coupled gas flow in coal seams during coal mining. Compared with the field observations, it may be suitable to use the stress sensitivity factor $\beta = 2.0$ for modeling the coupled gas flow in coal seams for the case study. Fig. 12 shows the gas permeability changes in the coal seam No C13 along the A–A′ section in Fig. 8 with different sensitivity parameter $\beta = 2.0$ and $\beta = 1.6$. Meanwhile, these results show that the in-situ stress in the coal seam No C_{13} is greatly decreased by mining the coal seam No B_{11}. Pressure relief and expansion deformation are induced by mining, and a large number of bed separation crannies are created in the coal seam No C_{13}. The field measurement results are in agreement with the numerical simulation.

4.4. Subsidence of the coal seam No C_{13} and associated gas flow

The simulated maximum subsidence of the coal seam are 1400 mm, 1500 mm, and 1600 mm as the working face advances 45 m, 70 m, and 100 m, respectively, and the range of the stress-relief zone in overburden strata is about 50 m. The numerical results agree well with the field observations depicted in Fig. 5.

Fig. 13 shows the change of the gas pressure in the coal seam No C_{13}. It can be seen that the gas pressure around the gas drainage boreholes sharply decreases from pre-drainage to post-drainage. For example, it decreases from 5 MPa at pre-drainage to 2.2 MPa at post-drainage after ten days' gas drainage and the working face's advances of 100 m. Moreover, the decreasing range of gas pressure gradually expands as the days of the gas drainage extends and the working face advances. The reason is that the coal seam No C_{13} above the goaf falls in the mining induced stress release zone, where the gas permeability of the coal seam remarkably increases, promoting the gas flow in coal seam and leading to an obvious decrease of the gas pressure around gas drainage boreholes. This is called the effect of reducing the stress to increase the permeability.

Compared with the field observations and the numerical results depicted in Figs. 7 and 13, respectively, there are some difference between the simulated results and the field observations. The differences are probably due to the 2D model simplification of the 3D case in practice and the assumed gas pressure of 25 kPa in the gas drainage boreholes. Anyway, the modeled dynamic process of the pressure relief gas drainage during coal mining on the whole agrees well with these in field observations.

4.5. Analyses and discussions

This paper revisited the engineering practices and conducted the numerical simulations for the long-distance pressure relief gas drainage in the coal seam No B_{11} at the PANYI coal mine, where there is nearly 70 m spacing between the coal seams No B_{11} and No C_{13}, and a relative coal seam distance of 35.

Through the fields observations, it was found that the gas pressure around the borehole in the coal seam No C_{13} decreased from 4.4 MPa to 0.4 MPa; the gas content in the coal seam No C_{13} decreased from 13 m^3/t to 5 m^3/t; the gas permeability of the coal seam No C_{13} increased from 2.84×10^{-4} mD to 0.817 mD by an increase of 2800 times; dilatational deformation of the coal seam No B_{11} reached up to 26.33‰; and the whole ratio of the gas emissions amount to above 60%. Comparing with some working faces without an application of the technique, the roadway driving speed in fully-mechanized long-

Table 1
Physical, mechanical and seepage parameters used in the numerical model.

No.	Lithology	Elastic Modulus E(GPa)	Uniaxial compressive strenth R_c(MPa)	Uniaxial tensile strength R_t (MPa)	Poisson Ratio λ	Friction angle (°)	Cohesion (MPa)	Layer thickness (m)
1	sandy mudstone	27.0	63	6	0.4	29	5.0	20.0
2	C_{13} coal seam	2	20	2	0.4	30	8	6.0
3	siltstnoe	31.1	60	6	0.27	30.5	9.4	6.0
4	siltstnoe	27.21	68	5	0.12	25.6	11.46	12.0
5	medium-grain sandstone	28.05	100.2	8	0.12	30.5	25.7	12.0
6	sandy mudstone	36.44	60	6	0.38	26.1	7.48	15.0
7	mudstone	27.58	86.5	4	0.21	20.9	10.68	4
8	fine sandstone	19.18	48.72	5	0.40	24.4	9.0	12.0
9	gritty mudstone	57.4.	30.61	3	0.26	37	4.8	6
10	B_{11b} coal seam	2	20	2	0.4	30	8	2
11	gritty mudstone	12.0	70	7	0.26	26	4.0	14

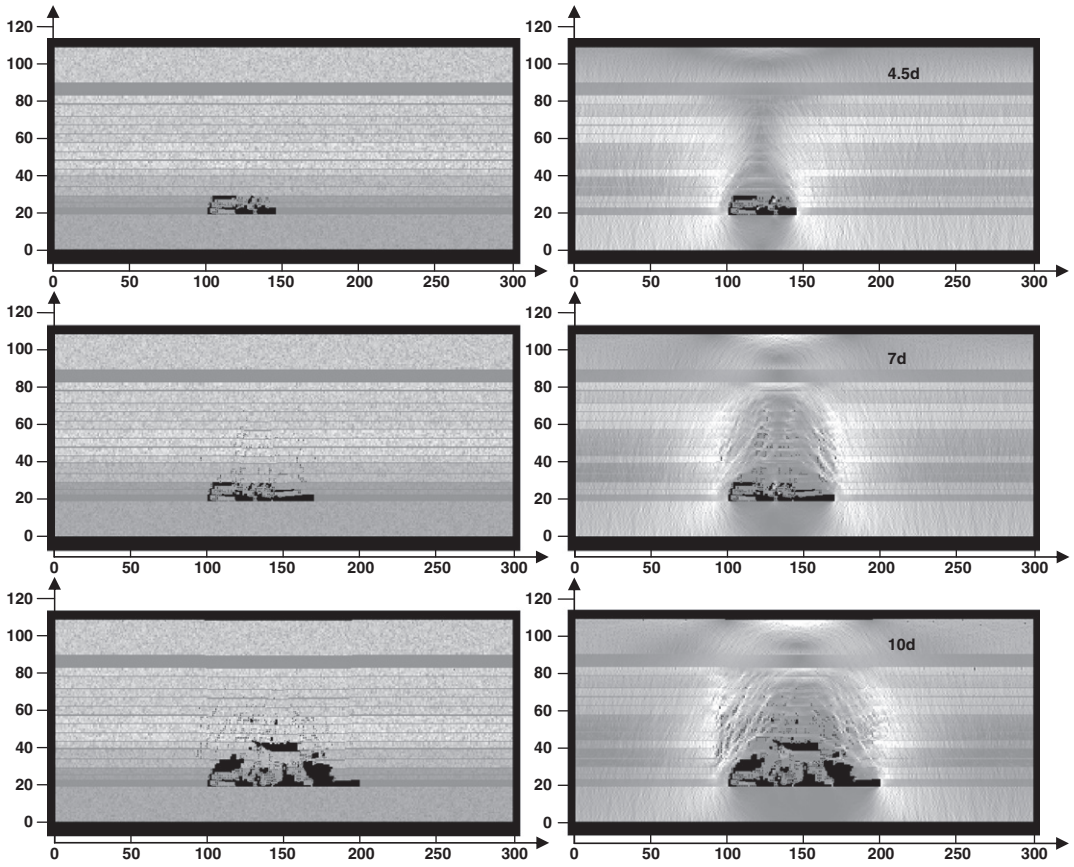

Fig. 9. Numerically simulated caving process of the strata and corresponding induced shear stress fields induced in the strata.

wall top coal caving mining zone increased from original 40–60 m per month to above 200 m per month. Moreover, the average production of the working face improved from 1700 tons/day to 5100 tons/day (i.e. with an increase of two times) and the relative gas emission of the heading face decreased from 25 m^3/min to 5.0 m^3/min (i.e. with an decrease of 5 times). Under equal air-conditions in the roadways, the average gas concentration in return airways decreased from 1.15% to 0.5%. In addition, the average monthly production of the working face can reach up to 7000 tons/day based on the current capacity of the gas drainage and the ventilation in the top caving working face.

The numerical simulations of the case study reproduced the mining induced deformation, subsidence and fracture characteristics of overburden strata, and the associated gas flow in the coal seam No C_{13}. Moreover, the numerical results revealed the effect of the in-situ stress on the gas permeability of the coal seam No C_{13}. According to

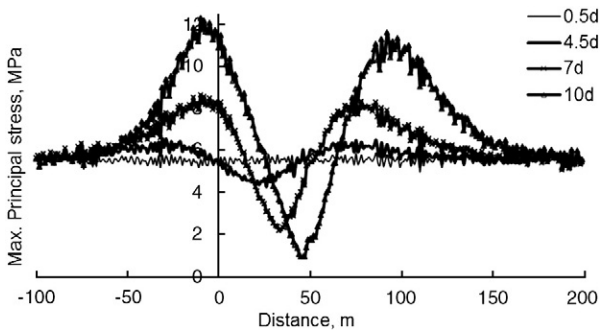

Fig. 10. Variation of the maximum principal stress in the coal seam No C_{13} due to the mining of the coal seam B_{11b} (AA′ section/m).

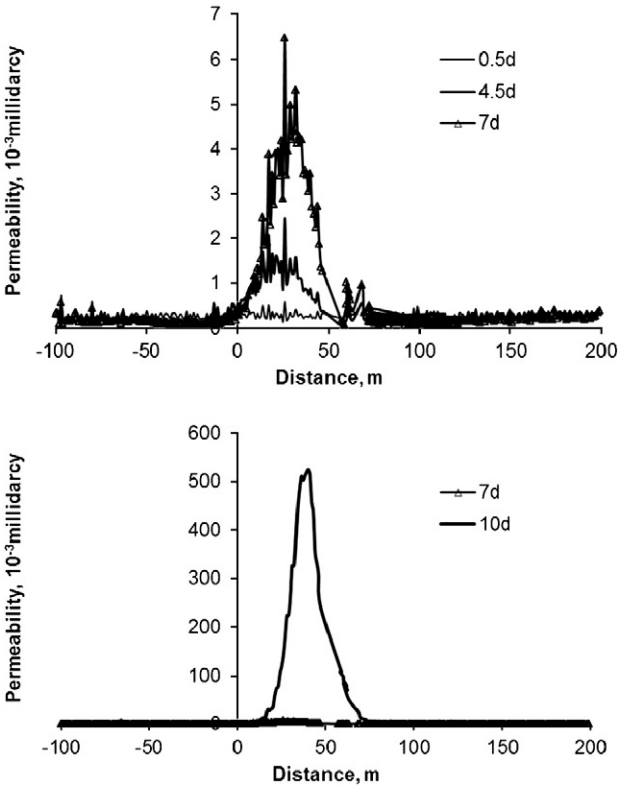

Fig. 11. Evolution of the gas permeability induced by mining (A–A′ section/m).

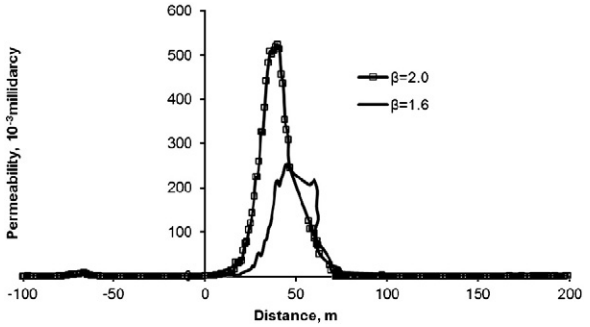

Fig. 12. Evolution of the gas permeability in the coal seam No C_{13} along the A–A′ section in Fig. 8 under different coupling parameters β.

the numerical simulations, the height of the caving zone is between 15 m and 20 m and the height of fractured zone is between 40 m and 45 m in the overburden strata above the B_{11} coal seam as the working face advances to about 100 m. Due to the extraction of the coal seam No B_{11}, the coal seam No C_{13} subsides on a whole in the mining induced sagging zone of the overburden strata. The modeled deformation of the coal seam is basically in accordance with that in field observations. When the working face is advanced to 10 days, an obvious increase of the gas permeability is observed in the horizontal range of up to 70 m in the coal seam No C_{13}. The magnitude of the gas permeability increase is up to about 2100 times higher than the initial gas permeability in the coal seam No C_{13}. The calculated increase is close to that observed in the field, which about 2800 times, considering the simplification in this paper and complex of the problem. The remarkable increase of the gas permeability indicated that the pressure relief and the expansion deformation are induced by coal mining and a large number of bed separations are created in the coal seam No C_{13}. In addition, the numerical results indicated that the gas pressure around the gas drainage boreholes sharply decreased from 5 MPa to 2.2 MPa after the gas drainage of ten days and the advance working face of 100 m. The decreasing range of the gas pressure gradually expanded as the gas drainage extends and the working face advances. Compared with the field observations and the numerical results in Figs. 7 and 13, respectively, there are some differences between the simulation and observations. It is concluded that the differences are probably caused by the 2D simplification of the 3D problem in practice and the assumption of the 25 kPa gas pressure in the gas drainage boreholes. Anyway, the modeled dynamic process of the pressure relief gas drainage during coal mining on the whole agrees well with these in field observations. Moreover, it was found that the gas pressure in the coal seam No B_{11} decreased from 4.4 MPa to 0.5 MPa; the gas content decreased from 13 m^3/t to 5 m^3/t; the gas permeability increased from 2.84×10^{-4} mD to 0.817 mD by an increase of 2880 times; the dilatational deformation reached up to 26.33‰; and the whole ratio of gas emissions amount to above 60%.

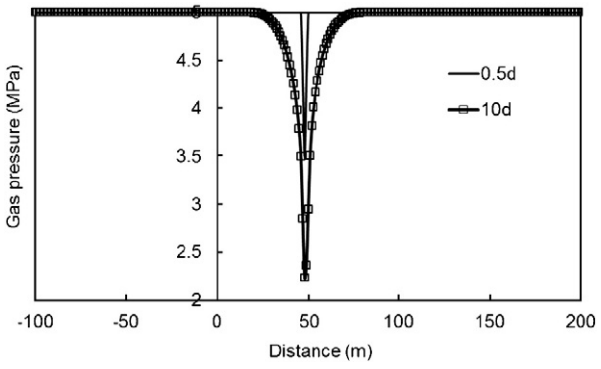

Fig. 13. Evolution of the gas pressure in the coal seam No C_{13} induced by mining.

Both the field observations and the numerical simulations revealed that the protective coal seam mining method should be adopted combining with the pressure relief gas drainage technique in high-gassy and outburst coal mine. As mentioned above, the method obviously eliminates the outburst hazard and also changes the coal seam No C_{13} from a high gas and outburst coal seam into a low non-outburst coal seam in the case study. Moreover, the method may lead to the high production and high-efficiency for high-gassy and outburst coal mine.

5. Conclusions

A mathematical model was proposed to simulate the deformation and fracture characteristics of overburden strata, the evolution of gas permeability, and the gas flow in protected coal seam, in which stress, damage, and seepage coupling are taken into accounted. In the case study, the engineering practice of the pressure relief gas drainage by mining protective coal seam was firstly revisited for the PANYI coal mine, which was owned by Huainan coal mining Co. Ltd. The numerical simulations were then performed to evaluate the effectiveness of the long-distance pressure relief gas drainage during extraction of protective coal seams at great depths. The numerical results visualized the three zones (i.e. caving, fractured and bending zones) in the overburden strata and three stress zones (i.e. stress concentration, stress relaxed and intact stress zones) in the protective coal seam induced by coal mining. The numerical simulations generally agree well with the field observations, especially, the increasing ratio of the gas permeability and the range of the pressure relief induced by the protective coal seam mining. Moreover, the numerical simulations indicate that the extraction of the coal seams causes the deformation, bed separation, and caving of overburden strata at a large scale, and the remarkable enhancement of the gas permeability of the protected coal seam, which in turn leads to obvious decrease of the gas pressure around boreholes in the surrounding rock mass. It is demonstrated that the technique of the pressure relief gas drainage by long-distance boreholes remarkably alleviates the risk of the coal and gas outbursts in the high-gassy coal seam of the low gas permeability, such as the coal seam No C_{13} in the case study. In addition, the technique also significantly reduces the gas content in the coal seam C_{13} and the gas emission in the working face. Correspondingly, a safe and high-efficient mining is secured in the main protected coal seam No C_{13}.

The numerical results offered some important theoretical indications of the mechanism of the gas flow in the coal seam. Furthermore, the results also provided some practical instructions of using the technique of the pressure relief gas drainage in the high-gassy coal seam of the low gas permeability to achieve the safe and high-efficient mining in fully-mechanized top coal caving and prevent the occurrences of the coal and gas outbursts in underground coal mining. Therefore, it is concluded that the model proposed in the paper is of significant help to deep the understanding of the gas flow mechanism in both theory and practice. It is pointed out that the long-distance pressure relief gas drainage technology can effectively improve the safety and productivity in underground coal mines, especially in the mining areas with the multiple high-gassy coal seams of the low permeability.

Acknowledgments

The work presented in this paper was financially jointly supported from the National Basic Research Program of China (2007CB209405), the Key Project of the National Natural Science Foundation of China (Grant No. 51034001, 50934006), the General Project of the National Natural Science Foundation of China (Grant

No. 10872046, 50874024), Doctoral Fund of Ministry of Education of China (No. 200801450003), Group Program (No. 90101001) of Northeastern University and the opening fund of State Key Laboratory of Geo-hazard Prevention and Geo-environment Protection, Chengdu University of Technology (SKLGP2010K008). Besides, the authors would like to thank the editor and the reviewers for their meticulous examinations, valuable comments and constructive suggestions on the manuscript.

Appendix A

Darcy's law describes fluid flow through a porous media, which can be expressed as

$$q = -\frac{kA}{\mu}\cdot\frac{dp}{dx} \tag{a.1}$$

where q is the volumetric flow, k is the permeability, μ is the viscosity, A is cross-sectional area, and dp/dx is the pressure gradient.

As for compressible ideal fluid, the change of density with pressure must be considered. According to the Boyle's law

$$p\cdot q\cdot t = p_a\cdot q_a\cdot t \tag{a.2}$$

where p and p_a are the gas pressure at a certain cross-section and outlet end of specimen, respectively. $q$and q_a are the volumetric flow at a certain cross-section and outlet end of specimen, respectively. t is the flow time.

Substitution of Eq. (a.2) into Eq. (a.1) yields

$$k\cdot A\cdot p\cdot dp = -\mu\cdot p_a\cdot q_a\cdot dx \tag{a.3}$$

Integration of Eq. (a.3) along the length of specimen yields

$$k\cdot A\cdot p\cdot\int_{p_1}^{p_a} dp = -\mu\cdot p_a\cdot q_a\cdot\int_0^L dx \tag{a.4}$$

in which p_1 is the gas pressure of the inlet end of the specimen and L is the length of the tested specimen.

The following Eq. (a.5) can be obtained from Eq. (a.4)

$$q_a = -\frac{kA}{2\mu\cdot p_a}\cdot\frac{dP}{dx} \tag{a.5}$$

Let $q_x = \frac{q_a}{A}$, $\lambda = \frac{k}{2\mu\cdot p_a}$, $P = p^2$, Eq. (a.5) becomes

$$q_x = -\lambda\cdot\frac{dP}{dx} \tag{a.6}$$

in which q_i is the flow velocity, λ is defined as the coefficient of gas filtration, and P is the square gas pressure.

Eq. (a.6) for two-dimensional or three-dimensional flow can be expressed in tensor form as

$$q_i = -\lambda_{ij}\cdot\frac{dP}{dn} \tag{a.7}$$

This is the generalization of *Darcy*'s law in terms of the square gas pressure.

References

Bauer, J., Lydzba, D., 1994. Model of gas–coal medium with a sorption phenomenon. Transport in Porous Media 14, 207–217.

Beamish, B.B., Crosdale, P.J., 1998. Instantaneous outbursts in underground coal mines: An overview and association with coal type. International Journal of Coal Geology 35, 27–55.

Chan, D.Y.C., Hughes, B.D., Paterson, L., 1993. Transient gas flow around boreholes. Transport in Porous Media 10, 137–152.

Chen, Y.P., Yu, Q.X., Yuan, L., 2004. Experimental research of safe and high-efficient exploitation of coal and pressure relief gas in long distance. Journal of China University of Mining & Technology 33, 132–136 (In Chinese with English abstract).

Connell, L.D., 2009. Coupled flow and geomechanical processes during gas production from coal seams. International Journal of Coal Geology 79, 18–28.

Connell, L.D., Detournay, C., 2009. Coupled flow and geomechanical processes during enhanced coal seam methane recovery through CO_2 sequestration. International Journal of Coal Geology 77, 222–233.

Hargraves, A.J., 1983. Instantaneous outbursts of coal and gas: A review. Proceedings of the Australian Institute of Mining and Metallurgy 285, 1–37.

Huainan Mining Group, C.L., 2002. Long-distance Pressure Relief Gas Drainage Technology in High Gassy and Low Permeable Soft and Thick Coal Seam. China University of Mining and Technology, Xuzhou. (in Chinese).

Hubbert, M.K., 1957. Darcy's law and the field equations of the flow of underground fluids. Hydrological Sciences Journal 2, 23–59.

Hyman, D.M., 1987. A Review of the Mechanisms of Gas Outbursts in Coal. US Department of the Interior, Bureau of Mines, IC 9155, Pittsburgh, PA. http://dx.doi.org/10.1080/02626665709493062.

Karacan, C.Ö., Diamond, W.P., Schatzel, S.J., 2007. Numerical analysis of the influence of in-seam horizontal methane drainage boreholes on longwall face emission rates. International Journal of Coal Geology 72, 15–32.

Lemaitre, J., Desmorat, R., 2005. Engineering Damage Mechanics. Springer-Verlag, Berlin.

Louis, C., 1974. Rock hydraulics. In: Muller, L. (Ed.), Rock Mechanics. Springer-Verlag, New York, pp. 287–299.

Lunarzewski, L.W., 1998. Gas emission prediction and recovery in underground coal mines. International Journal of Coal Geology 35, 117–145.

Noack, K., 1998. Control of gas emissions in underground coal mines. International Journal of Coal Geology 35, 57–82.

Otuonye, F., Sheng, J., 1994. A numerical simulation of gas flow during coal/gas outbursts. Geotechnical and Geological Engineering 12, 15–34.

Pan, Z., Connell, L.D., 2009. Comparison of adsorption models in reservoir simulation of enhanced coalbed methane recovery and CO_2 sequestration in coal. International Journal of Greenhouse Gas Control 3, 77–89.

Paterson, L., 1986. A model for outbursts in coal. International Journal of Rock Mechanics and Mining Sciences & Geomechanics Abstracts 23, 327–332.

Schneider, T., Preuße, A., 1995. Recovery and utilisation of coal seam gas — impetus by the German hard coal mining industry. Erdöl Erdgas Kohle 111, 515–519.

Shepherd, J., Rixon, L.K., Griffiths, L., 1981. Outbursts and geological structures in coal mines: A review. International Journal of Rock Mechanics and Mining Sciences & Geomechanics Abstracts 18, 267–283.

Sun, P.D., Wan, H.G., 2004. A coupled model for solid deformation and gas leak flow. International Journal for Numerical and Analytical Methods in Geomechanics 28, 1083–1104.

Tang, C.A., Tham, L.G., Lee, P.K.K., Yang, T.H., Li, L.C., 2002. Coupled analysis of flow, stress and damage (FSD) in rock failure. International Journal of Rock Mechanics and Mining Sciences 39, 477–489.

Terzaghi, K., Peck, R.B., Mesri, G., 1996. Soil Mechanics in Engineering Practice. John Wiley & Sons, New York.

Valliappan, S., Zhang, W.H., 1996. Numerical modelling of methane gas migration in dry coal seams. International Journal for Numerical and Analytical Methods in Geomechanics 20, 571–593.

Valliappan, S., Zhang, W.H., 1999. Role of gas energy during coal outbursts. International Journal for Numerical Methods in Engineering 44, 875–895.

Viete, D.R., Ranjith, P.G., 2006. The effect of CO_2 on the geomechanical and permeability behaviour of brown coal: Implications for coal seam CO_2 sequestration. International Journal of Coal Geology 66, 204–216.

Xu, T., Tang, C.A., Yang, T.H., Zhu, W.C., Liu, J., 2006. Numerical investigation of coal and gas outbursts in underground collieries. International Journal of Rock Mechanics and Mining Sciences 43, 905–919.

Xu, T., Yan, A., Hao, T., Yu, S., 2007. Numerical modeling of cross measure borehole gas drainage. In: Jin, G., Zhou, A., Gao, J., et al. (Eds.), Progress in Mining Science and Safety Technology. Science Press, Beijing, pp. 1358–1363.

Yang, T.H., Tang, C.A., Xu, T., Rui, Y.Q., 2004. Seepage Characteristic in Rock Failure. Science Press, Beijing. (in Chinese).

Yu, Q.X., Chen, Y.P., Jiang, C.L., 2004. Principles and applications of exploitation of coal and pressure relief gas in thick and high-gas seams. Journal of China University of Mining & Technology 33, 127–131 (In Chinese with English abstract).

Yu, S.B., 1992. One-dimensional flow model for coal–gas outbursts and initiation criterion. Acta Mechanica Sinica 8, 363–373 (In Chinese with English abstract).

Zhao, C., Valliappan, S., 1995. Finite element modelling of methane gas migration in coal seams. Computers & Structures 55, 625–629.

Zhou, S.N., Lin, B.Q., 1998. The Theory of Gas Flow and storage in Coal Seams. China Coal Industry Publishing House, Beijing. (in Chinese).

Zhu, W.C., Liu, J., Sheng, J.C., Elsworth, D., 2007. Analysis of coupled gas flow and deformation process with desorption and Klinkenberg effects in coal seams. International Journal of Rock Mechanics and Mining Sciences 44, 971–980.